

1 **Footshock-induced activation of the claustrum-entorhinal** 2 **cortical pathway in freely moving mice**

3

4 Wushuang HUANG^{1,#}, Jing QIN^{1,#}, Chunqing ZHANG², Han QIN^{3,*}, Peng XIE^{1,*}

5 ¹Department of Neurology, The First Affiliated Hospital of Chongqing Medical University,
6 Chongqing, 400016, China; NHC Key Laboratory of Diagnosis and Treatment on Brain Functional
7 Diseases, Chongqing Medical University, Chongqing, 400016, China, ² Department of Neurosurgery,
8 Xinqiao Hospital, Army Medical University, 183 Xinqiao Main Street, Shapingba District, Chongqing
9 400037, China, ³Center for Neurointelligence, School of Medicine, Chongqing University,
10 Chongqing 400044, China.

11

12 Corresponding author: Peng Xie, Department of Neurology, The First Affiliated Hospital of
13 Chongqing Medical University, Chongqing, 400016, China; NHC Key Laboratory of Diagnosis and
14 Treatment on Brain Functional Diseases, Chongqing Medical University, Chongqing, 400016, China.

15 E-mail: xiepeng@cqmu.edu.cn.

16 Han Qin, Center for Neurointelligence, School of Medicine, Chongqing University, Chongqing
17 400044, China. E-mail: qinhan@cqu.edu.cn.

18

19 [#]Wushang Huang and Jing Qin contributed equally to this work.

20 ^{*}Peng Xie and Han Qin are co-corresponding authors.

21

22 Short title: Footshock-induced activation of the CLA-MEC pathway

23

24

25 **Summary**

26 Footshock is frequently used as an unconditioned stimulus in fear conditioning behavior studies.
27 The medial entorhinal cortex (MEC) contributes to fear learning and receives neuronal inputs from
28 the claustrum. However, whether footshocks can induce a neuronal response in claustrum-MEC
29 (CLA-MEC) projection remains unknown. Here, we combined fiber-based Ca²⁺ recordings with a
30 retrograde AAV labeling method to investigate neuronal responses of MEC-projecting claustral
31 neurons to footshock stimulation in freely moving mice. We achieved successful Ca²⁺ recordings in
32 both anesthetized and freely exploring mice. We found that footshock stimulation reliably induced
33 neuronal responses to MEC-projecting claustral neurons. Therefore, the footshock-induced
34 response detected in the CLA-MEC projection suggests its potential role in fear processing.

35

36 **Keywords**

37 Claustrum • Fear • Footshock • Fiber photometry • GCaMP

38

39 **Introduction**

40 Fear, which can elicit defensive behaviors to avoid or reduce harm, is an important emotion for
41 survival [1, 2]. Fear is regulated by multiple brain regions and complex neural circuits. The amygdala
42 nuclei are essential for the acquisition and expression of fear [3, 4]. Fear responses are involved in
43 dispersed brain networks, such as the sensory cortex, the medial prefrontal cortex, the
44 hippocampus and the entorhinal cortex [1, 5]. Footshock-induced pain is frequently used as the
45 unconditioned stimulus in fear conditioning experiment paradigms [4, 6]. The claustrum, a slender
46 region underneath the cortical area, has a neuroanatomical basis that allows it to participate in
47 high-order functions [7, 8]. The medial entorhinal cortex (MEC), which has been reported to
48 participate in fear learning, receives neuronal projections from the claustrum [9-11]. Thus, the
49 neuronal projection from the claustrum to the MEC (CLA-MEC) may be involved in fear processing
50 [9]. However, whether footshock can induce any response in the CLA-MEC projection remains
51 unknown.

52 Real-time monitoring approaches are needed to answer this question. Traditional
53 electrophysiological recording provides the highest temporal resolution in neural activity recording.
54 Combined with optogenetics, optrodes provide cell-type or projection information for recorded

55 neurons [11-14]. However, the application of this technique is limited by a low recording efficiency.
56 Two-photon microscopy provides a high recording efficiency but is restricted to cortical areas in
57 anesthetized or head-fixed animals [15, 16]. Fiber photometry combined with genetically encoded
58 Ca^{2+} indicators provides a simple but efficient method for projection-specific recording in freely
59 moving animals [17, 18]. Recent studies have developed recording methods in the claustrum in
60 freely moving mice [19, 20]. However, the real-time recording of a specific CLA-MEC projection
61 under specific behavioral tasks is still lacking.

62 Here, we utilized fiber-based Ca^{2+} recording to investigate the possible role of the CLA-MEC
63 projection in footshock-induced neural responses. We observed a stable labeling of MEC projection
64 neurons in the claustrum by local injection of retrograde AAV carrying the Ca^{2+} indicator GCaMP6m
65 gene into the MEC. The method was then validated by Ca^{2+} recording in anesthetized and freely
66 moving mice. Moreover, we performed Ca^{2+} recording of MEC projection neurons in the claustrum
67 with the application of footshock stimuli in freely moving mice. Robust neuronal responses of these
68 neurons to footshock stimuli were observed, suggesting a possible role of CLA-MEC projection in
69 fear-related information processing.

70

71 **Methods**

72 **Animals**

73 Eleven adult male C57BL/6J mice (aged between 8-12 weeks) were used for all described studies.
74 Mice were housed in groups under 12-hour light/dark cycle conditions, with *ad libitum* access to
75 food and water. All experiments were performed according to institutional animal welfare
76 guidelines and were approved by the Third Military Medical University Animal Care and Use
77 Committee.

78

79 **Optical setup**

80 A custom-built fiber photometry system was used to record Ca^{2+} activity. Excitation light with a
81 wavelength of 488 nm (Coherent, OBIS 488 LX-50 mW) was delivered to tissue by an optical fiber
82 with a diameter of 200 μ m (Doric Lenses, MFP_200/230/900-0.48). The optical fiber was glued into
83 a short metal cannula (ID. 0.51 mm, OD. 0.82 mm, length 18 cm) with a fiber tip extending \sim 3.5
84 mm out of the cannula. Emission fluorescence was detected with an avalanche photodiode

85 (Hamamatsu Photonic, Si APD, S2382). Data acquisition was controlled by user-customized
86 software on the LabVIEW platform (LabVIEW 2014, National Instruments).

87

88 **Virus injection**

89 The mice were anesthetized with 1.5% isoflurane in pure oxygen for 3-5 min. mice were then
90 moved onto a stereotactic apparatus with a heating pad that maintained a temperature of
91 approximately 37 °C during the entire surgery, and anesthesia was maintained by continuous
92 delivery of isoflurane. The hair at the top of the head was shaved, and an 8-10-mm-long incision
93 was made along the midline. Then, one small craniotomy (0.5 × 0.5 mm) above the MEC (AP: -4.9
94 mm, ML: 3.5 mm) was made. A glass micropipette with a tip diameter of ~10 μm was inserted
95 down to a depth of 2.5 mm (from the dura) to infuse the virus. Approximately 300 nL of retroAAV-
96 GCaMP6m viral solution was gradually injected while the micropipette was slowly lifted to a depth
97 of 1.5 mm. Each injection took 5-10 min. The micropipette was kept in place for 5 min before being
98 slowly withdrawn. After virus injection, the scalp wound was closed with surgical sutures, and each
99 mouse was kept in a warm plate. Mice were then returned to their home cage for recovery.
100 Meloxicam oral suspension (Metacam) was provided in drinking water for three days after surgery.

101

102 **Fiber recording in anesthetized mice**

103 Recording experiments were conducted approximately one month after virus injection. The
104 preprocessed fiber probe was slowly inserted through another craniotomy above the claustrum
105 (AP: 1.1 mm, ML: 2.5 mm) to a depth of ~2.7 mm. After the fiber probe was secured to the skull by
106 UV-curing hardening dental cement (Tetric EvoCeram, 595953WW), the concentration of isoflurane
107 was increased to 1.8%. Following an adaptation period of 10 min, Ca²⁺ recordings were performed
108 for 10 min at each anesthesia level, and the initial 3 min of each level was excluded for data analysis.
109 The concentrations of isoflurane were 1.8%, 1.5%, 1.2%, and 0.8%.

110

111 **Fiber recording in freely moving mice**

112 The cannula was fixed to the mouse skull with dental cement after recording data from the mice
113 in an anesthetized state, and then the mice were returned to their home cages for recovery.
114 Meloxicam oral suspension (Metacam) was provided in drinking water immediately after surgery

115 for three days. Freely moving mice were placed into an opaque plastic rectangular box (30 cm × 17
116 cm) for 30 min. Ten sound stimulation trials (8944 Hz pure tone, 1 s, 70 dB sound pressure level, 3
117 min inter-sound interval) were played for mice. Subsequently, mice were moved to an electric
118 shock box (50 cm × 50 cm) for 10 footshock trials (1 s, 0.6 mA, 3 min inter-shock interval). In the
119 meantime, a camera was set above the recording box to monitor the behaviors of the mice. Ca²⁺
120 signals and mouse behaviors were recorded simultaneously. Event markers were used to
121 synchronize the Ca²⁺ signals and behavior videos.

122

123 **Histology and imaging**

124 All experimental mice were perfused after recording to confirm the virus expression areas and fiber
125 positions. Mice were perfused with phosphate-buffered saline (PBS) for ~ 5 min and then with 4%
126 paraformaldehyde for 15-20 min to ensure complete tissue fixation. Brain samples were collected
127 and placed in 4% paraformaldehyde overnight at 4 °C. Brain tissue was sectioned into 50- μ m-thick
128 slices with a freezing microtome and then stained with 4',6-diamidino-2-phenylindole (DAPI).
129 Fluorescent images were collected with a fluorescent microscope using a 2.5 \times or 4 \times objective.

130

131 **Data analysis and statistics**

132 The Ca²⁺ data were acquired at a sampling rate of 2000 Hz and analyzed as previously described
133 [18, 21, 22]. A Savitzky–Golay finite-impulse smoothing filter (50 side points and 3 polynomial
134 orders) was first applied to the data. Then, the relative fluorescence change was calculated by $\Delta f/f$
135 = $(f - f_{\text{baseline}})/f_{\text{baseline}}$, where f_{baseline} was the baseline fluorescent intensity. A transient was identified
136 as a Ca²⁺ event if the amplitude was three times larger than the standard deviation of the baseline
137 segment.

138 Nonparametric and 1-way ANOVA with *post hoc* Tukey's multiple comparisons tests in
139 MATLAB (MATLAB 2016b, MathWorks) were used for comparison. All summarized data were from
140 individual mice and plotted as the mean \pm SEM.

141

142 **Results**

143 **Specific labeling of claustral neurons that project to the MEC by GCaMP6m**

144 We used the fiber photometry system [18, 21, 22] to monitor the population Ca²⁺ activity of
145 claustral neurons that project to the MEC (CLA^{MEC}-projecting neurons, Fig. 1a). We expressed the

146 genetically encoded Ca²⁺ sensor GCaMP6m [23] specifically in CLA^{MEC}-projecting neurons by
147 injecting retroAAV-syn-GCaMP6m [24] into the MEC (Fig. 1b,c). Then, an optical fiber was
148 implanted above the claustrum to record the Ca²⁺ activity from CLA^{MEC}-projecting neurons (Fig. 1b,
149 d). The expression of GCaMP6m was verified and was restricted in the MEC by *post hoc* histology
150 (Fig. 1e). Robust expression of GCaMP6m in the claustrum was also confirmed (Fig. 1f).

151

152 **Population Ca²⁺ recordings of MEC-projecting claustral neurons in anesthetized mice**

153 Next, we determined whether the Ca²⁺ signals in the claustrum could be recorded by optical fibers
154 with our labeling method. The Ca²⁺ signals of CLA^{MEC}-projecting neurons were recorded under
155 different anesthesia levels by isoflurane. Figure 1g shows examples of Ca²⁺ signals from CLA^{MEC}-
156 projecting neurons at decreasing anesthesia levels (1.8%, 1.5%, 1.2%, and 0.8%). We observed slow
157 oscillation-associated population Ca²⁺ events, similar to the observations that have been previously
158 described in the cortex [21, 25-27], in CLA^{MEC}-projecting neurons. The amplitude and frequency of
159 the Ca²⁺ events changed with different anesthesia levels. The amplitude ($\Delta f/f$) decreased from 0.13
160 ± 0.05 to 0.05 ± 0.01 when the isoflurane concentration decreased from 1.8% to 0.8% (Fig. 1h,
161 repeated measures 1-way ANOVA with Tukey's multiple comparisons test, $F = 16.37$, 1.8% vs. 0.8%,
162 $P = 0.006$; 1.5% vs. 0.8%, $P = 0.0002$; 1.2% vs. 0.8%, $P = 0.007$). Meanwhile, the frequency increased
163 from 0.36 ± 0.05 Hz to 3.29 ± 0.35 Hz under these conditions (Fig. 1i, repeated measures 1-way
164 ANOVA with Tukey's multiple comparisons test, $F = 37.27$, 1.8% vs. 1.5%, $P = 0.03$; 1.8% vs. 1.2%, P
165 $= 0.00004$; 1.8% vs. 0.8%, $P = 0.00003$, 1.5% vs. 1.2%, $P = 0.004$; 1.5% vs. 0.8%, $P = 0.002$). Thus,
166 the retrograde labeling method can be combined with fiber photometry for real-time neural
167 activity recording of CLA^{MEC}-projecting neurons.

168

169 **Population Ca²⁺ response in MEC-projecting claustral neurons induced by footshock in freely 170 behaving mice**

171 To investigate the response induced by footshock in freely moving mice, we conducted optical fiber
172 recordings of CLA^{MEC}-projecting neurons together with behavioral video surveillance. We
173 performed the recordings at least 5 days after fiber implantation. Mice were placed in a white
174 rectangular box for free exploration, with an infrared camera placed above them to monitor their
175 behavior (Fig. 2a). Figure 2b shows a 200-s recording of Ca²⁺ signals (black trace) synchronized with
176 body movements (gray trace). Mouse locations during the corresponding recording period were

177 automatically tracked and are plotted in Figure 2c. According to both the example in Figure 2b and
178 statistical analysis in Figure 2d, we found significantly higher Ca^{2+} signals during locomotion than
179 during grooming behavior (Fig. 2d, two-sided Wilcoxon rank-sum test, $z = 6.3$, $p = 2.88\text{e-}10$).

180 We next performed fiber recordings of CLA^{MEC} -projecting neurons during the application of
181 sound or footshock in freely moving mice (Fig. 2e). We found that sound stimulation could not
182 induce any Ca^{2+} signal (four example trials from one mouse in Figure 2f, left; summary of 19 trials
183 from 3 mice in Fig. 2g), while footshock stimulation induced clear and stable responses from
184 CLA^{MEC} -projecting neurons (four example trials from one mouse in Fig. 2f, right; summary of 21
185 trials from 3 mice in Fig. 2h). The onset latency of these footshock-induced Ca^{2+} responses was 48.3
186 ± 4.8 ms (21 trials from 3 mice). The peak amplitude ($\Delta f/f$) of footshock-induced Ca^{2+} responses
187 was significantly larger than that of sound stimulation (Fig. 2i, two-sided Wilcoxon rank-sum test, z
188 $= 5.3$, $p = 1.28\text{e-}7$).

189

190 Discussion

191 In this study, we utilized fiber photometry to investigate the neural responses in CLA-MEC
192 projection to footshock stimulation. We used a retrograde AAV carrying the genetically encoded
193 Ca^{2+} indicator GCaMP6m to specifically label MEC-projecting neurons in the claustrum. To test the
194 effectiveness of the retrograde labeling, we first performed Ca^{2+} recording in the anesthetized state
195 by implantation of an optical fiber probe in the claustrum of retroAAV-GCaMP6m-injected mice.
196 We found that the amplitude of the population Ca^{2+} events decreased with decreasing isoflurane
197 concentration. In contrast, the frequency increased in this process. Then, we demonstrated Ca^{2+}
198 recordings of CLA^{MEC} -projecting neurons in freely moving mice. Stable neuronal responses induced
199 after footshock but not sound stimulation were detected in the CLA^{MEC} -projecting neurons. These
200 Ca^{2+} responses after footshock could result from locomotion, pain sensation or startle reflex caused
201 by footshock [28]. Future work is needed to differentiate these possibilities.

202 The claustrum has been hypothesized to be involved in higher-order processes, depending on
203 its dense connection to and from the associative cortex [9, 10, 29, 30]. Moreover, it has been
204 suggested to participate in multiple brain functions, such as sensory information integration,
205 attention and consciousness [29-32]. The projection from the claustrum to MEC has been less
206 studied. Kitanishi et al. reported that CLA-MEC projection was activated by novel context and

207 modulated contextual memory [9]. However, the real-time activity pattern of CLA-MEC projection
208 has not been clearly investigated. Here, we showed that a fiber-based recording method combined
209 with retrograde AAV labeling can achieve real-time recording of specific projections in freely
210 behaving mice, which will aid our understanding of the function of specific neural projections.

211 Overall, we demonstrated that fiber-based Ca^{2+} recording combined with retrograde AAV
212 labeling is ideal for real-time monitoring of CLA-MEC projection in freely moving mice. With this
213 approach, we found a stable and reliable response of CLA^{MEC}-projecting neurons induced by
214 footshock stimulation. These findings may lead to a clearer understanding of neural circuits in fear
215 learning and pain.

216

217 **Acknowledgments**

218 The authors are grateful to Ms. Jia Lou for help in composing and editing the layout of the figures.
219 This work was supported by grants from the National Natural Science Foundation of China
220 (82171463) to CZ.

221

222 **Conflicts of interest**

223 There are no conflicts of interest.

224

225 **References**

- 226 1. Tovote P, Fadok JP, Lüthi A. Neuronal circuits for fear and anxiety. *Nat Rev Neurosci.*
227 2015;16(6):317-331.
- 228 2. Garcia R. Neurobiology of fear and specific phobias. *Learn Mem.* 2017;24(9):462-471.
- 229 3. LeDoux JE. Emotion circuits in the brain. *Annu Rev Neurosci.* 2000;23:155-184.
- 230 4. LeDoux J. The amygdala. *Curr Biol.* 2007;17(20):R868-874.
- 231 5. Wahlstrom KL, Huff ML, Emmons EB, Freeman JH, Narayanan NS, McIntyre CK, LaLumiere
232 RT. Basolateral amygdala inputs to the medial entorhinal cortex selectively modulate the
233 consolidation of spatial and contextual learning. *J Neurosci.* 2018;38(11):2698-2712.
- 234 6. Phillips RG, LeDoux JE. Differential contribution of amygdala and hippocampus to cued and
235 contextual fear conditioning. *Behav Neurosci.* 1992;106(2):274-285.
- 236 7. Jackson J, Smith JB, Lee AK. The anatomy and physiology of claustrum-cortex interactions.
237 *Annu Rev Neurosci.* 2020;43:231-247.
- 238 8. Smith JB, Lee AK, Jackson J. The claustrum. *Curr Biol.* 2020;30(23):R1401-r1406.
- 239 9. Kitanishi T, Matsuo N. Organization of the claustrum-to-entorhinal cortical connection in
240 mice. *J Neurosci.* 2017;37(2):269-280.
- 241 10. Zingg B, Dong H-W, Tao HW, Zhang LI. Input–output organization of the mouse claustrum.
242 *J Comp Neurol.* 2018;526(15):2428-2443.
- 243 11. Narikiyo K, Mizuguchi R, Ajima A, Shiozaki M, Hamanaka H, Johansen JP, Mori K, Yoshihara
244 Y. The claustrum coordinates cortical slow-wave activity. *Nat Neurosci.* 2020;23(6):741-

245 753.

246 12. Anikeeva P, Andalman AS, Witten I, Warden M, Goshen I, Grosenick L, Gunaydin LA, Frank
247 LM, Deisseroth K. Optetrode: a multichannel readout for optogenetic control in freely
248 moving mice. *Nat Neurosci.* 2011;15(1):163-170.

249 13. Stark E, Koos T, Buzsaki G. Diode probes for spatiotemporal optical control of multiple
250 neurons in freely moving animals. *J Neurophysiol.* 2012;108(1):349-363.

251 14. Chevée M, Finkel EA, Kim SJ, O'Connor DH, Brown SP. Neural activity in the mouse
252 claustrum in a cross-modal sensory selection task. *Neuron.* 2022;110(3):486-501.e487.

253 15. Denk W, Strickler JH, Webb WW. Two-photon laser scanning fluorescence microscopy.
254 *Science.* 1990;248(4951):73-76.

255 16. Yuste R, Denk W. Dendritic spines as basic functional units of neuronal integration. *Nature.*
256 1995;375(6533):682-684.

257 17. Adelsberger H, Garaschuk O, Konnerth A. Cortical calcium waves in resting newborn mice.
258 *Nat Neurosci.* 2005;8(8):988-990.

259 18. Qin H, Fu L, Hu B, Liao X, Lu J, He W, Liang S, Zhang K, Li R, Yao J et al. A visual-cue-
260 dependent memory circuit for place navigation. *Neuron.* 2018;99(1):47-55.e44.

261 19. White MG, Panicker M, Mu C, Carter AM, Roberts BM, Dharmasri PA, Mathur BN. Anterior
262 cingulate cortex input to the claustrum is required for top-down action control. *Cell Rep.*
263 2018;22(1):84-95.

264 20. White MG, Mu C, Qadir H, Madden MB, Zeng H, Mathur BN. The mouse claustrum is
265 required for optimal behavioral performance under high cognitive demand. *Biol Psychiatry.*
266 2020;88(9):719-726.

267 21. Zhang Q, Yao J, Guang Y, Liang S, Guan J, Qin H, Liao X, Jin W, Zhang J, Pan J et al.
268 Locomotion-related population cortical Ca(2+) transients in freely behaving mice. *Front*
269 *Neural Circuits.* 2017;11:24.

270 22. Qin H, Lu J, Jin W, Chen X, Fu L. Multichannel fiber photometry for mapping axonal terminal
271 activity in a restricted brain region in freely moving mice. *Neurophotonics.* 2019, 6(3):1-
272 10, 10.

273 23. Chen TW, Wardill TJ, Sun Y, Pulver SR, Renninger SL, Baohan A, Schreiter ER, Kerr RA, Orger
274 MB, Jayaraman V et al. Ultrasensitive fluorescent proteins for imaging neuronal activity.
275 *Nature.* 2013;499(7458):295-300.

276 24. Tervo DG, Hwang BY, Viswanathan S, Gaj T, Lavzin M, Ritola KD, Lindo S, Michael S,
277 Kuleshova E, Ojala D et al. A designer aav variant permits efficient retrograde access to
278 projection neurons. *Neuron.* 2016;92(2):372-382.

279 25. Luczak A, Bartho P, Marguet SL, Buzsaki G, Harris KD. Sequential structure of neocortical
280 spontaneous activity in vivo. *Proc Natl Acad Sci USA.* 2007;104(1):347-352.

281 26. Stroh A, Adelsberger H, Groh A, Ruhlmann C, Fischer S, Schierloh A, Deisseroth K, Konnerth
282 A. Making waves: initiation and propagation of corticothalamic Ca²⁺ waves in vivo. *Neuron.*
283 2013;77(6):1136-1150.

284 27. Adelsberger H, Grienberger C, Stroh A, Konnerth A. In vivo calcium recordings and
285 channelrhodopsin-2 activation through an optical fiber. *Cold Spring Harb Protoc.*
286 2014;2014(10):pdb prot084145.

287 28. Zhang K, Förster R, He W, Liao X, Li J, Yang C, Qin H, Wang M, Ding R, Li R et al. Fear learning
288 induces $\alpha 7$ -nicotinic acetylcholine receptor-mediated astrocytic responsiveness that is

289 required for memory persistence. *Nat Neurosci.* 2021;24(12):1686-1698.

290 29. Liu J, Wu R, Johnson B, Vu J, Bass C, Li J-X. The claustrum-prefrontal cortex pathway
291 regulates impulsive-like behavior. *J Neurosci.* 2019;39(50):10071-10080.

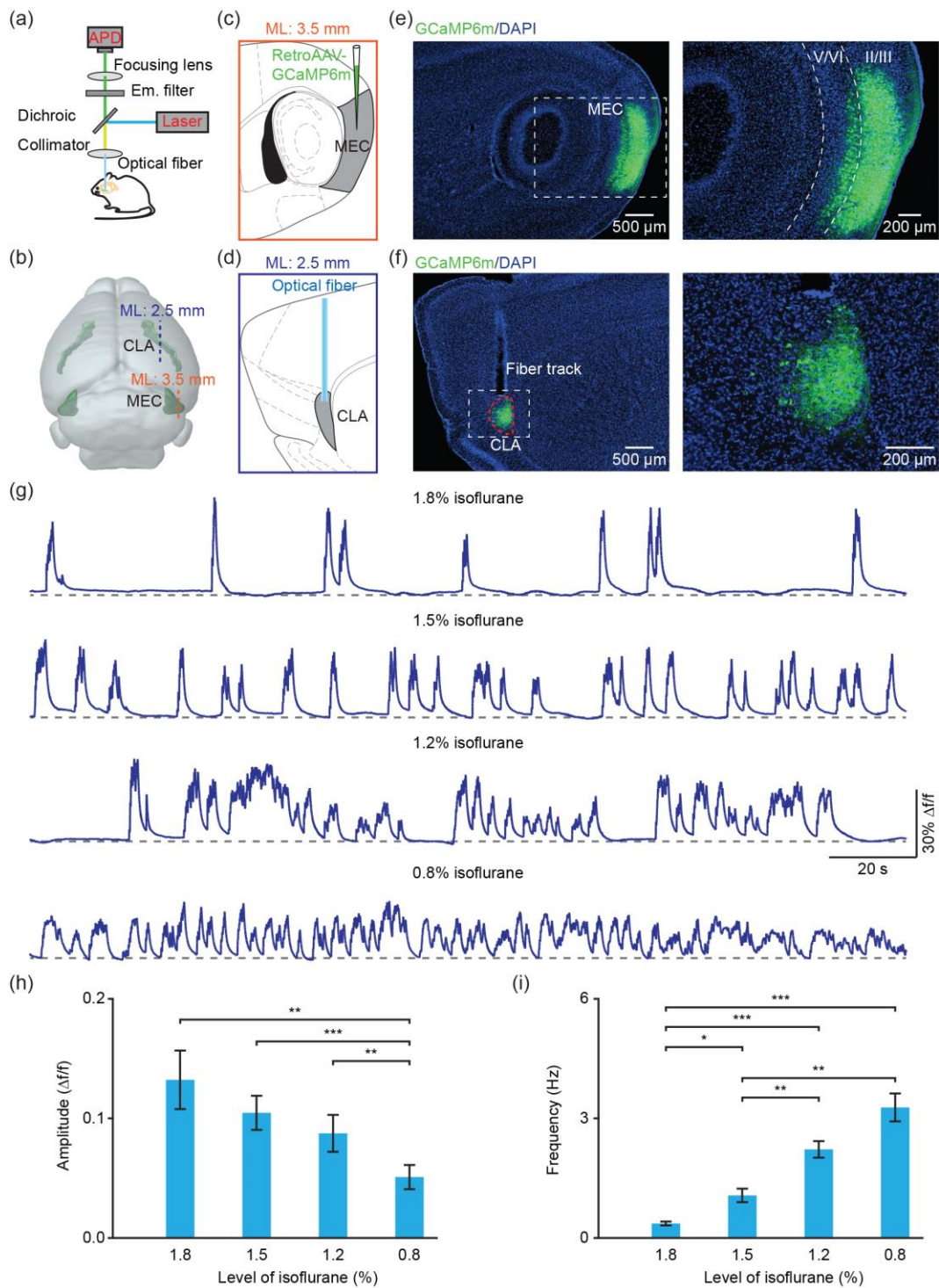
292 30. Terem A, Gonzales BJ, Peretz-Rivlin N, Ashwal-Fluss R, Bleistein N, Del Mar Reus-Garcia M,
293 Mukherjee D, Groysman M, Citri A. Claustral neurons projecting to frontal cortex mediate
294 contextual association of reward. *Curr Biol.* 2020;30(18):3522-3532.e3526.

295 31. Atlan G, Terem A, Peretz-Rivlin N, Sehrawat K, Gonzales BJ, Pozner G, Tasaka G-I, Goll Y,
296 Refaeli R, Zviran O et al. The claustrum supports resilience to distraction. *Curr Biol.*
297 2018;28(17):2752-2762.e2757.

298 32. Jackson J, Karnani MM, Zemelman BV, Burdakov D, Lee AK. Inhibitory control of prefrontal
299 cortex by the claustrum. *Neuron.* 2018;99(5):1029-1039.e1024.

300

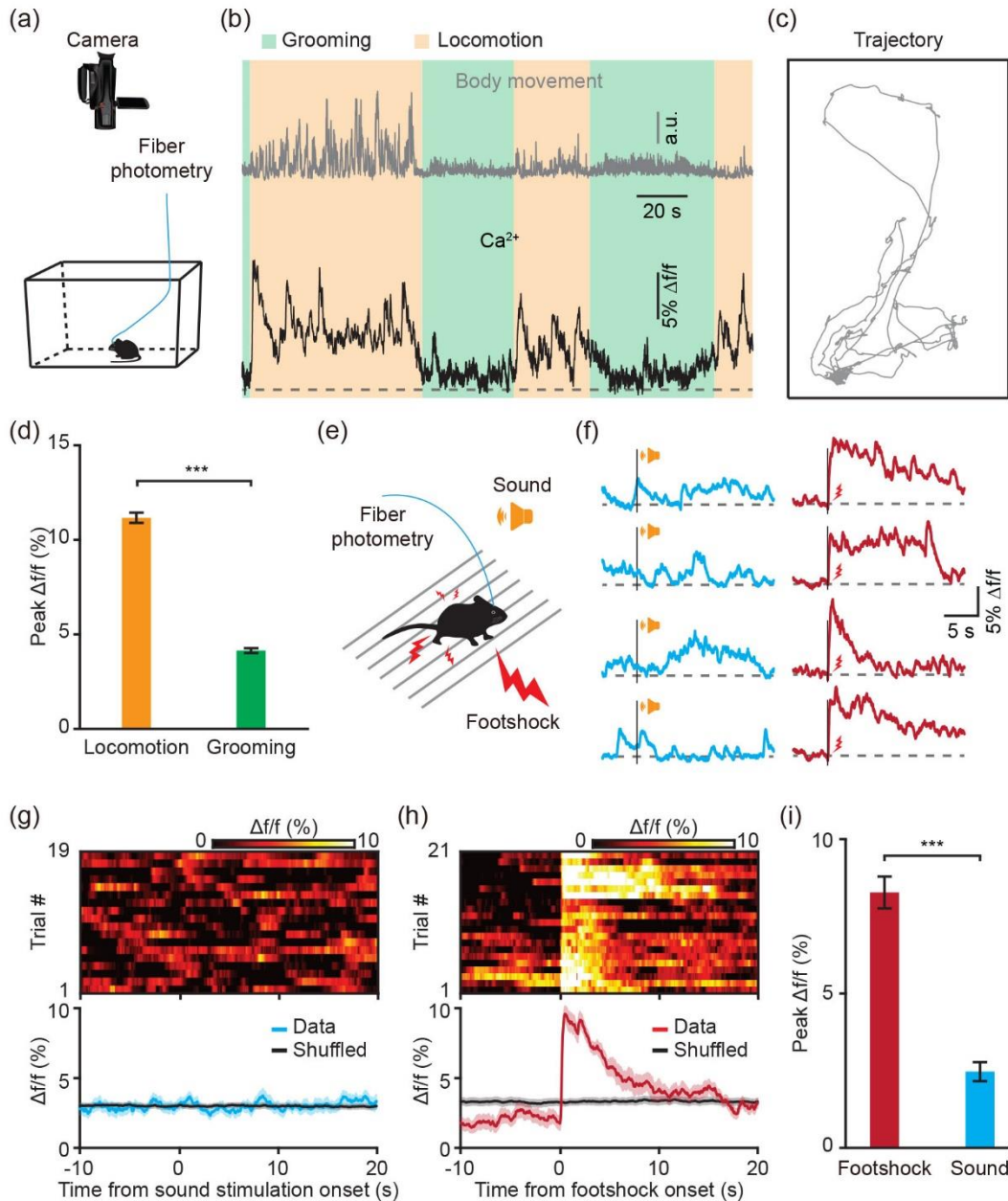
301



303

304 **Figure 1** Population Ca^{2+} recordings of CLA^{MEC} -projecting neurons in anesthetized mice with
 305 GCaMP6m. (a) Schematic of the fiber photometry setup. (b-d) Experimental design of retroAAV-
 306 GCaMP6m injection in the MEC (c) and fiber implantation in the claustrum (d); ML: mediolateral,
 307 CLA: claustrum; MEC: medial entorhinal cortex. (e) *Post hoc* histological images showing the
 308 expression of GCaMP6m in the MEC. (f) *Post hoc* histological confirmation of GCaMP6m expression
 309 and optical fiber position in the claustrum. (g) Examples showing the population Ca^{2+} signals of
 310 CLA^{MEC} -projecting neurons at different anesthesia levels. (h) Amplitude of Ca^{2+} events of CLA^{MEC} -

311 projecting neurons at different anesthesia levels ($n = 11$ mice; repeated measures 1-way ANOVA
 312 with Tukey's multiple comparisons test, $**P < 0.01$, $***P < 0.001$). (i) Frequency of Ca^{2+} events of
 313 CLA^{MEC} -projecting neurons at different anesthesia levels ($n = 11$ mice; repeated measures 1-way
 314 ANOVA with Tukey's multiple comparisons test, $*P < 0.05$, $**P < 0.01$, $***P < 0.001$)
 315



316

317 **Figure 2** Population Ca^{2+} transients of CLA^{MEC} -projecting neurons induced by footshock stimulation
 318 in freely moving mice. (a) Diagram of the recording setup in freely moving mice. (b) Example
 319 showing the relative body movements (gray trace) and the Ca^{2+} transients recorded in CLA^{MEC} -
 320 projecting neurons (black trace) in a freely moving mouse; green shaded areas: grooming; yellow
 321 shaded areas: locomotion. (c) The corresponding locomotion trajectory of the recording period in
 322 b. (d) Summary of peak $\Delta f/f$ during locomotion or grooming (locomotion: $n = 31$ trials from 3 mice;
 323 grooming: $n = 24$ trials from 3 mice, two-sided Wilcoxon rank-sum test, $***p < 0.001$). (e) Schematic
 324 diagram of Ca^{2+} recording with footshock or sound stimulation. (f) Representative Ca^{2+} signals

325 induced after sound (blue) or footshock (red) in CLA^{MEC}-projecting neurons from one mouse. (g, h)
326 Color-coded intensities (top) and average trace (bottom) of Ca²⁺ signals aligned to sound (g, 19
327 trials from 3 mice) or footshock (h, 21 trials from 3 mice) stimulation. The black trace is the shuffled
328 data, and shaded areas represent s.e.m. (i) Summary of peak $\Delta f/f$ during sound and footshock
329 stimulation (sound: $n = 19$ trials from 3 mice, footshock: $n = 21$ trials from 3 mice, two-sided
330 Wilcoxon rank-sum test, $z = 5.1$, $***p < 0.001$).
331